RC23072 (W0401-099) January 20, 2004
Other

IBM Research Report

Molecular Dynamics Investigation of the Structural Properties of Phosphatidylethanolamine Lipid Bilayers

Mike C. Pitman, Frank Suits
IBM Research Division
Thomas J. Watson Research Center
P.O. Box 218
Yorktown Heights, NY 10598

Scott Feller
Department of Chemistry
Wabash College
Crawfordsville, Indiana 47933

Research Division
Almaden - Austin - Beijing - Haifa - India - T. J. Watson - Tokyo - Zurich

Molecular Dynamics Investigation of the Structural Properties of Phosphatidylethanolamine Lipid Bilayers

Michael C. Pitman,* Frank Suits,* and Scott E. Feller†

*IBM T. J. Watson Research Center, Yorktown Heights, New York 10598 USA; and †Department of Chemistry, Wabash College, Crawfordsville, Indiana 47933 USA

ABSTRACT We report a 14ns microcanonical (NVE) molecular dynamics simulation of a fully hydrated bilayer of 1-stearoyl-2-oleoyl-phosphatidyethanolamine (SOPE). This study describes the structure of the bilayer in terms of NMR order parameters and radial distribution functions, and compares them to experimental results and simulations of other lipids. A focus of this work is the characterization of the lipid-water interface, particularly the hydrogen bonding network of the phosphatidylethanolamine (PE) headgroups. We find that hydrogen bonding between the primary amine and phosphate groups has a pronounced effect on the structure of PE relative to phosphatidylcholine (PC), and is evident in the P-N radial distribution functions.

INTRODUCTION

Phosphatidylethanolamine (PE) plays a role in a wide variety of biological functions including cell division (Emoto and Umeda, 2000, Emoto *et al*, 1996), membrane fusion (Teague *et al*, 2002), vesicle formation (Birner et al. 2001), growth

(Storey et al, 2001), reproduction (Martinez and Morros, 1996), and motility (Kearns 2001). Although the abundance of PE is highly variable across organisms and cell types (Henneberry et al, 2002, Dowhan, 1996), it contributes as much as 70% of the membrane composition in bacteria such as E. Coli (Dowhan, 1997). PE is often distributed across the cell membrane asymmetrically and is often concentrated in the inner leaflet of the membrane. The PE headgroup is generally paired with two fatty acid acyl chains and in animal tissues shows a preference for polyunsaturated fatty acids, such as arachidonic and docosahexaenoic, as compared to PC lipids.

A well-studied property of PE is its ability to form inverse hexagonal phases (H_{II}), which play an important role in membrane fusion mechanisms (Rappolt et al. 2003, Jahn and Grubmüller, 2002, Kozlov, 1994) and vesicle formation (Birner et al. 2001). In contrast to the more abundant phosphatidylcholines (PC), PE has a primary amine that allows it to form strong hydrogen bonds, both to its own phosphate group and to neighboring phosphates. These hydrogen bonds are responsible for an increase in transition temperatures for PE relative to PC (Blume, 1980), and may play an important role in many of its unique properties. In addition, the primary amine gives PE a reduced headgroup size compared to PC, which may cause the relative stability of the $L\alpha$ to H_{II} phase (Kozlov, 1994), particularly in the presence of cholesterol (Marinov and Dufourc, 1996). The reduced headgroup size also affects how PE packs in mixtures of other lipids and with cholesterol; cholesterol has been found to reduce the transition temperature by as much as 20 ˚C for inverse hexagonal phase formation (Paré and Lafleur, 1998). Hydration of the PE headgroup is also significantly different from PC, with measurements of the hydration force between bilayers showing a factor of two difference in the number of solvent molecules taken up in multilamellar dispersions (Rand and Parsegian, 1989).

Molecular dynamics simulations of SOPE bilayers provide a view not only of structural properties that can be matched to experiment, but also of the hydrogen bond

networks that play a role in their lateral organization. Model membranes of saturated and unsaturated asymmetric substitution are interesting in terms of biological relevance (Henneberry et al, 2002). Asymmetrically substituted lipids, in particular lipids with saturated chains in the *sn*-1 and unsaturated chains in the *sn*-2 position, have distinct trends in the order parameter profiles of the saturated chain compared to the di-saturated chain (Seelig and Seelig, 1977). One focus of this study is to investigate whether this trend emerges in molecular dynamics simulation and to discuss its possible origins. Although the study reported here is confined to the structural properties determined from simulation, a later work will report dynamical behavior that is also accessible via molecular dynamics.

METHODS

Our intent was to investigate the structural and dynamical properties of an SOPE bilayer. Although dynamical data is best extracted from an NVE ensemble to avoid artifacts introduced by temperature and pressure control algorithms (Moore et al, 2001, Allen and Tildesley, 1987), structural data is often derived from constant temperature and pressure (NPT) ensembles under the assumption that structural properties are less sensitive to ensemble-induced artifacts than the dynamical properties. However, if an NVE simulation is stable enough in temperature and pressure to perform a valid long trajectory, it can provide data for both structure and dynamics. It has been shown that artifacts may result in lipid bilayer simulations as a consequence of inappropriate densities (Feller et al., 1997). Methods for applying constant surface tension as well as constant normal pressure with constant surface area have been investigated (Feller et al.,

1999), with the conclusion that an appropriate constant surface area can alleviate the need to specify an applied surface tension. Our simulations were done with Blue Matter (Fitch et al., 2003), the molecular dynamics software developed for the Blue Gene project (Allen et al., 2001), which performed NVE runs of the SOPE system that were sufficiently stable to yield data for both the structural and dynamical investigations. We therefore performed all our simulations entirely in NVE, while the system preparation involved stages of NPT. After sufficient equilibration with NPT, a volume as close to the mean volume was chosen for NVE production.

We obtained the initial structure from a previously equilibrated bilayer of 72 POPC molecules, which served as a template for the SOPE system. We constructed the SOPE bilayer by adding a methyl and methylene groups to the end of the palmitoyl chains and removing the choline methyl groups of the POPC bilayer. We then hydrated the system to approximately 20 waters per lipid.

We used the following protocol to obtain an appropriate density. The deuterium order parameters and the area per lipid are related, but the experimental uncertainty of the area per lipid is much higher than that of the deuterium order parameter profiles (Petrache et al., 1999). We therefore used the mean deuterium order parameter of the stearoyl chain as the guide to the bilayer density and made a series of anisotropic adjustments to the system, followed by NPT equilibration, until we achieved an average order parameter that was reasonably close to experiment. Since the template structure was an equilibrated POPC bilayer, which has an area per lipid much higher than SOPE, we had to compress the initial system laterally. In order to do this without inducing excessive Van der Waals forces that would result from a simple lateral rescaling, we performed an iterative

stretch/equilibration process in the following manner: With the bilayer normal oriented along the z-axis, we scaled the unit cell z-dimension and all z-coordinates by 3-5%, then allowed it to relax under conditions of isotropic pressure control set to 1 atm. The adjustment of the system's normal-to-lateral aspect ratio under isotropic pressure control provided a lateral compression force as the water restored its model specific density (TIP3P, in this case). After several hundred picoseconds of equilibration we examined the order parameter profile to gauge the area per lipid relative to the experimental target. When we measured a deficiency in the area per lipid compared to the experimental target, we scaled up the X and Y dimensions accordingly. We repeated this process until we achieved an average order parameter value close to the experimental value. After a final 1.2 ns of NPT equilibration, we brought the system into a microcanonical ensemble for production.

For our simulations we used the all-atom CHARMM force field for lipids (Feller and MacKerell, 2000). All equilibration and production runs of SOPE system were performed with Blue Matter on an IBM SP2 (450MHz power3) cluster running 32-way with a 2 fs timestep and a P3ME grid spacing of 0.5 Å. The production runs averaged 1 ns of simulation time every 4 days.

Results and Discussion

Simulation Stability

The total energy and the temperature over the 14 ns production run is shown in Figure 1. The stability evident on the multi-nanosecond timescale alleviates the need for temperature control and allows both structural and dynamical information to be extracted from the same trajectory. This stability is encouraging in light of an aggressive 2fs timestep with standard Verlet integration. Long term oscillations in temperature with a multi-nanosecond period are evident, and any upward trend in temperature that may be present is not distinguishable from these longer period oscillations.

The plot of total energy during the simulation shows the small drift of only 0.04 Kcal/mol per ns. The temperature trace during the simulation shows that kinetic energy is also stable during the simulation, with a drift of 0.06 K per ns. Inspection of the temperature trace also reveals long term oscillations with multi-nanosecond periods. The slope of the trend line is also sufficiently low that it is indistinguishable from long term oscillations. Based on the stability of temperature and energy during these multi-nanosecond trajectories, we conclude that the long term heating is small compared to the inherent long term variation in temperature, and the trajectories are suitable for both structural and dynamical measurements.

Bilayer structure

Experimentally, the area per lipid, A_L, is notoriously difficult to measure with a high precision (Nagle, 1993). A common means of estimating A_L is through its relation to the averaged chain orientational order parameter, S_{av} (Petrache et al., 1999). Using this method, SOPE in 4/4/1 mixtures of 18:0-18:1 PC/PE/PS (Huster et al., 2000), has an estimated area per lipid of 59.2 $Å^2$, as calculated from S_{av} = 0.182 at 30 °C. Pure PE at

35 ˚C has S_{av} = 0.217, with an estimated A_L of 57.9 Å^2 (Huster et Al., 1998). Following the protocol described in the methods section for obtaining the appropriate density, and therefore $A_{L,}$ we arrived at $A_{L\,=}$ 58.1 Å^2 for a simulation temperature of 37 ˚C. This value is intermediate to pure PE at 35 ˚C and a mixture of PC/PE/PS at 30 ˚C. S_{av} over the 14 ns was fairly constant at 0.201.

Electron density distribution of selected groups

Figure 2 shows the electron density distribution along the bilayer normal. We computed electron density distributions by scaling the number densities of selected groups by the appropriate electron count of those groups. We averaged the number densities from samples taken every 100 ps over the 14 ns of simulation time.

The total electron density distribution is similar in form to that of DOPC as determined by a joint neutron and x-ray refinement method (Weiner and White, 1992). The phosphate, methylene, olefin, terminal methyl and water show a high degree of similarity. The overlap of the terminal methyl groups with the acyl region is consistent with experiment and simulation, indicating transfer of magnetization from the terminal methyl to the methylenes at the C2 position (Huster et al. 1999).

Examination of infrared C=O stretching (Paré and Lafleur, 1998) indicates a substantial degree of hydration of POPE with the C=O . This is consistent with the substantial overlap with the water and acyl regions of the density distribution.

Order parameter profiles

The order parameter S_{CD} is a measure of orientational order of the acyl chains. S_{CD} is obtained experimentally from the quadrupolar splittling $\Delta\nu_Q$, using the relation $\Delta\nu_Q$ = ¾$(e^2qQ/h)S_{CD,}$ where (e^2qQ/h) is the quadrupolar coupling constant measured directly in NMR experiments. In a simulation the orientational order parameter profile is

$$S_{CD}(n) = 1/2\left\langle 3\cos^2\beta_n - 1\right\rangle, \qquad (1)$$

where β_n is the angle between a C-H bond vector and the bilayer normal. Values generally fall in the range of 0 to -0.4, and are reported as $-S_{CD}$ or $|S_{CD}|$.

As noted in the setup protocol, we used the relationship of the S_{av} to A_L (Area per lipid) (Petrache et al., 1999) to set the appropriate surface density. We adjusted the surface density with stages of scaling and isotropic NPT equilibration until S_{av} was sufficiently close to experiment. Since adjustments to the surface density caused consistent shifts in the order parameter profile without affecting the relative order of individual carbons, the shape of the profile was insensitive to S_{av} and A_L.

Figure 3 compares the stearoyl chain to the selectively deuterated palmitoyl chain of POPC (Seelig and Seelig, 1977), with experimental values shown as the dark filled squares; the simulated values are shown as open squares with error bars. We compared the palmitoyl chain (16 carbons) to the stearoyl chain (18 carbons) in the following manner: We aligned the plateau region (carbons 2 through carbon 6) and separately aligned the tail regions (stearoyl carbons 10-17 are aligned to palmitoyl carbons 8-15), since the chain dynamics near the tails are most appropriately compared. We computed the uncertainty using snapshots 5ps apart over the 14ns of the simulation (5 ps is assumed to be statistically independent). The experimental values of POPC that appear in the figure were taken 19 ˚C above the gel to liquid crystalline transition temperature (-5 ˚C

for POPC). The effect of increased order around C6 measured in POPC is temperature dependent, being most pronounced at temperatures close to the gel to liquid crystalline phase transition, and flattening out at higher temperatures. The transition temperature of SOPE is 30˚C (Huster et al., 1998). For our simulation temperature of 37˚C, or 7˚C above the transition temperature, we expected to see a fairly pronounced maximum. However, a strict comparison to a corresponding 7 ˚C above the transition temperature of POPC may not be optimal; SOPC has a transition temperature of 3˚C (Phillips et al,1972), hence the increase of transition temperature due to the increased chain length is relatively minor. Much of the increase in transition temperature is due to hydrogen bonding of PE (Blume, 1980). For example, the transition temperature for POPE is 20˚C (Epand and Bottega, 1987). The comparison to POPC 19˚C above its transition temperature is therefore appropriate.

The trend of orientational order going through a maximum around C6 has been attributed to the double bond of the oleoyl chain (Seelig and Seelig, 1977), which would make that trend unexpected in measurements of disaturated lipids. The trend of decreasing order near the headgroup has been reported in other simulations of SDPC and PDPC (Saiz and Klein, 2001a, Saiz and Klein, 2001b, Huber et al., 2002, Böckmann et al., 2003), but the trend for those systems has received less discussion in the literature.

There is a significant departure from experiment for S_{CD} at the C2 position of the stearoyl chain. Figure 3 shows that the SOPE simulated value is more disordered than the selectively deuterated C2 position of POPC (0.18 for SOPE compared to 0.22 for POPC). In a closer examination, Figure 4 shows a histogram of S_{CD} values for the C2 carbon. The bulk of the values are in a reasonable range ($S_{CD} \sim -0.2$), yet two outliers have highly

disordered values (S_{CD} = +0.4). These two lipids held their high values over the full 14 ns of simulation time. As will be shown in the dynamics paper, headgroups are sufficiently slow that several tens of nanoseconds of simulation may be required to completely equilibrate circumstances in the headgroup region. This is a point of concern when using a method of order parameters that considers the time average of individual lipids as an unbiased sample. In the present case, that would assign a weight of 2/144 (two cases for the 144 methylene hydrogens at the stearoyl C2 position). If we drop the outliers from the analysis, $|S_{CD}|$ at the C2 position moves up to a value of 0.19. The overall distribution is fairly skewed toward disorder, but the mode of the distribution is in good correspondence with experiment. Aside from the C2 position, the quantitative agreement for SOPE and POPC is significant, since only the S_{av} of the stearoyl chain was brought close to its experimental value by the choice of surface area (see methods) while the quantitative agreement of the shape of the entire profile is obtained for both the stearoyl and oleoyl chains.

For the oleoyl chains, shown in Figure 5, the selectively deuterated data for POPC (Seelig and Seelig, 1977, Seelig and Waespe-Šarčević, 1978) shows a disordered trend around the double bond. The simulation data is consistent with this trend, as well as other reported simulations (Huber et al. 2002, Mashi et al., 2001). There is a notable departure from experiment in the C2 position of the oleoyl chain. Oleoyl chain positions C3-C7 and C13 to the tail were not selectively deuterated and there values are not available. The S_{CD} values for C3-C7 and C13-C18 are similar for the stearoyl and oleoyl chains. The region near the double bond has good agreement with experiment.

Amine-Phosphate Coordination and hydrogen bond network structure

A property that distinguishes PE from PC is its ability to form strong hydrogen bonds between the phosphate and the primary amine, and the degree of hydrogen bonding in the L_α fluid phase at biologically relevant temperature is a focus of this study. Experimentally, the amine-phosphate dipoles are parallel to the membrane surface (Brown and Seelig, 1978), consistent with the electron density distributions in Figure 3, showing that the density for the amine and phosphate groups occupies the same region with respect to the bilayer normal. Furthermore, sub-zero deuterium NMR studies of DOPE hydration as a function of increasing methylation of the amine imply a role for the extended hydrogen bonding capability of the primary amine, since it would explain the different phase behavior of phospholipids with different degrees of methylation (Hsieh and Wu, 1995).

Figure 6 shows the two dimensional intermolecular phosphorous-nitrogen radial distribution functions (RDF) for SOPE and POPC. In contrast to PC, the first two layers are more highly structured. The degree of structure from the RDF's implies that neighboring headgroups are clustered together much more so than in PC. The 2^{nd} and 3^{rd} peaks in the first shell take on larger distances, presumably due to strain energy through the ethanolamine chain. Inspection of the full P-N RDF shows the first shell is composed of three peaks, only one of which appears in the intermolecular 2D RDF. The two other peaks unique to intramolecular P-N interactions occur at slightly larger distances,

presumably due to internal strain energy from ring closure of the ethanolamine to form hydrogen bonds with the distinct phosphate oxygens.

Figure 7 shows the 3D radial distribution of both P-H_2O and N-H_2O for SOPE. Structure in the water surrounding the primary amine groups is apparent out to three solvation shells. Order between water and phosphate groups is not substantially different from random beyond the first solvation shell. Both phosphate and amine groups compete for hydrogen bonds to water and to each other. There is relatively small overlap of the amine and acyl chain carbonyl group distributions (see Figure 2), which also offers h-bonding possibilities to the amines, implying acyl-amine coordination is much less likely.

The hydrogen bonds have been shown to be responsible for the higher transition temperatures measured for PE relative to PC (Blume 1980). Figure 8 shows a surface region that exhibits an extended network of h-bonds. The blue-stripped tubes depict the hydrogen bonds, according to the DSSP definition (Kabsch and Sander, 1983) commonly used for protein secondary structure assignment (amine-carbonyl backbone h-bonds). The tube thickness is related to the strength of the hydrogen bond. It is notable that uncoordinated, mono-, bi-, and trifurcated hydrogen bonds are present for the amines. For the phosphate groups, we see oxygens with bifurcated hydrogen bonds, as well as bi-dentate coordination to the phosphate group. We suggest that the ability of PE to form such an extensive array of hydrogen bonding patterns, due to its primary amine, may be responsible for many of its unique properties. The extensive hydrogen bond networks that

result from the particularly high level of coordination may have implications for properties that occur on much larger length scales that what we have investigated here.

Compressibility modulus

Lateral compressibilities are fairly well characterized for a variety of PCs (Petrache et al. 2000, Rawicz et al. 2000); PE's, however, have received somewhat less attention. The distribution of areas per lipid has been used to estimate the lateral compressibility modulus for DPPC in a variety of ensembles (Feller and Pastor 1999). It was found that estimating the compressibility through fluctuations gave estimates about a factor of four too high, which implies the fluctuations were too small by a factor of two for DPPC (Feller and Pastor 1999). Estimates between ensembles at an appropriate applied surface tension were shown to be consistent with estimates from constant surface area simulations. Such a method should be applicable to our NVE simulation, in light of the agreement with the order parameter profile, implying that the overall density is correct.

Methods for estimating the distribution of areas per lipid via Voronoi tessellation have been developed (Weiss et al. 1995, Shinoda and Okazaki 1998, Allen and Tildsley 1987). Figure 9 shows the area per lipid distribution computed from Voronoi cells. Voronoi tessellation was done in two ways: projecting the center of mass (COM) of the whole lipid (COM_{SOPE}) onto the plane of the bilayer, and a second set from projecting the COM of only the phosphoethanolamine region of the headgroup (COM_{PE}) onto the plane of the bilayer. The latter is useful for analysis of the head group organization discussed below, but we were interested to compare the two distributions in light of the potential

artifacts resulting from the use of $COM_{SOPE;}$ in particular, the distribution of chain conformations may have a complicated effect of the COM projection when chains adopt laterally extended conformations (in principle it is possible for projected COM of neighboring lipids to be coincident).

The distribution was computed using snapshots 50ps apart over the 14ns of simulation time, using the COM of each lipid. The mean for COM_{SOPE} is 58.2 $Å^2$ with σ = 14.8; the mean for tessellating with just the PE is necessarily the same, while σ = 22.4, implying a lower compressibility modulus. These values correspond to a lateral compressibility modulus of $K_{A(SOPE)}$ = 113 dyn/cm and $K_{A(PE)}$ = 49.8 dyn/cm. Note the distributions are skewed toward higher areas ($skew_{SOPE}$ = 0.80, $skew_{PE}$ = 1.16).

Lateral Organization

We have used the Voronoi tessellation of the phosphoethanolamine portion of the headgroup to help understand the lateral organization. Figure 10 shows the Voronoi tessellation for the center of mass of the phosphoethanolamine groups for a sample snapshot. To show the neighborhood of the boundary regions for each edge of the simulation cell, nine simulation cells are shown. Previous studies define the coordination number as the sum of the sides of a given Voronoi cell. Since some cells have a mixture of long and short edges, we instead used the fractional coordination number,

$$\chi = \pi / \arccos(2A/RP) \qquad (2)$$

defined by Weiss (Weiss et al., 1995). In this expression, A is the area of the polygon, R is the mean distance to the verticies, and P is the perimeter. This definition has the

advantage of weighting edges appropriately based on their sizes relative to the cell, while still providing the expected value for regular polygons. The color coding in Figure 10 indicates this fractional coordination number for each cell, and one can see that regions of high and low head group density show marked lateral organization. Note that ridges (bands of high headgroup density) generally extend into the symmetry-related neighboring cells, suggesting order on a scale larger than the simulation cell. Although the snapshot tessellated in Figure 10 is representative of the structural motifs found throughout the 14ns, the lateral organization is fairly dynamic, and can change rapidly in terms of cluster configuration with minimal lateral diffusion. Many local coordination motifs show stability on the multi-nanosecond timescale, while bridges between clusters were seen to form and dissociate on the nanosecond to sub-nanosecond time scale.

In Figure 11, we take a closer look at the hydrogen bonding networks that underlie the lateral organization apparent in Figure 10. Figure 11 shows a time average of the phosphate (red) and nitrogen (green) positions over the 100 ps time window matching the Voronoi tessellated configuration shown in Figure 10. The tubes connecting each phosphate distribution with a corresponding nitrogen distribution indicate the P-N pairs in the same lipid. The extent of the red and green regions depicts the corresponding positional distribution over a 100ps time frame. Four simulation cells are shown. Hydrogen bond networks between amine and phosphate groups are clearly seen from the patterns of alternating red and green density clouds. Over this time window an individual lipid near the lower right corner (and its three symmetry equivalents) can be seen in an unbound migratory state where the N distribution is bimodal and the P distribution is relatively diffuse. Just above this migratory lipid, other motifs such as ladders and rings

are apparent, as well as centrally radial configurations. The variety of lipid configurations that arise from higher order hydrogen bonding configurations is rich and warrants further investigation. It is clear from the present work that a proper characterization of the structural variety will require a larger simulation cell, due to interference from imposed symmetry of the boundary conditions, and the propensity for lateral organization on at least the multi-nanometer length scale. We can, however, focus on the sub-nanometer details that support this structural variety.

Figure 12 shows an atomic view of the headgroups corresponding to Figures 10 and 11. Here, the atoms of the phosphatidylethanolamine are shown with explicit hydrogen bonds rendered with blue-striped cylinders. A study of the intricacies of the hydrogen bonding patterns antecedent to the lateral organization shown in Figures 10 and 11, as well as Figure 8, reveals a high level of coordination for the amine and phosphate groups. Note that even the migratory lipid discussed in Figure 11 is seen in Figure 12 to form intramolecular hydrogen bonds. Ring motifs can be seen to form with a variety of hydrogen bond patterns. Clusters are seen to form from many possible hydrogen bonding patterns. The dynamics of these motifs will be the subject of a future work.

Conclusion

We have characterized the structure of SOPE in terms of electron density distributions with respect to the bilayer normal, chain order via deuterium order parameters, and the lipid-water interface in terms of radial distribution functions. The electron density distributions are not very distinct and have many common features across a variety of lipids. The order parameter profiles agreed quantitatively with analogous selectively

deuterated chains. The unique trend of order going through a maximum around C6 of the saturated chain when in the presence of an unsaturated chain in the sn-2 position did emerge in the simulation. This is an encouraging example of how simulation may assist with peak assignments in NMR experiments. The quantitative agreement in the shapes of both the stearoyl and oleoyl chains between a PE (from simulation) and PC (from Seelig and Seelig, 1977) headgroup suggests the headgroup does not impose specific structural constraints on the fatty acid chains, i.e. the effect of headgroup on chain structure is general one acting through the change in surface area requirement. The nitrogen-phosphorous, nitrogen-H_2O, and phosphorous-H_2O radial distribution functions revealed structure consistent with extensive hydrogen bonding. Close inspection of the coordinated structures revealed a rich dynamic of binding modes, include mono-, bi-, and tri-furcated hydrogen bond of the amine to neighboring phosphates, and high order coordination of phosphates to several amine groups. Although ridges and clusters of coordinated amine-phospate hydrogen bonded networks were observed to form and dissociate over the 14ns simulation, the length scale was such that the symmetry imposed by the periodic boundary conditions constrained their true extent. A more complete characterization of the extended hydrogen bond networks will require a large simulation cell, and likely longer simulation time.

The success of Blue Matter to conduct, to our knowledge, the longest stable NVE simulation of a system of this size, was key to our work. The stability of the simulation enables structural and dynamical information to be extracted from a single trajectory without perturbations from temperature control methods altering the inherent dynamics of

the system. We find the stability given the 14 ns duration encouraging for much longer simulations where dynamical information is of interest.

This is the first study to directly investigate the unique order parameter profile that results from a mixed saturated and unsaturated lipid since it was first observed through selective deuteration (Seelig and Seelig, 1977). The quantitative agreement of the order parameter profiles shows that the profile is reproducible with constant volume and energy simulations once the appropriate density is attained using the averaged order parameter available from NMR experiments, using the protocol described in the methods section. These results are in support of simulation, offering assistance in understanding experimental data.

Finally, we note this is one of the first multi-nanosecond simulations of a mixed saturated and mono-unsaturated phosphatidylethanolamine system, a biologically relevant major membrane component that has received relatively little attention. In this work we have focused on structural properties SOPE. Future work will focus on chain and headgroup dynamics.

ACKNOWLEDGEMENTS

The authors would like to acknowledge the fine work and support of the Blue Matter Team – Blake G. Fitch, Robert. S. Germain, Alex Rayshubskiy, T. J. Chris Ward, Yuri Zhestkov, Maria Eleftheriou, Jed W. Pitera, and William C Swope. We also extend a special thanks to Klaus Gawrisch for many insightful discussions.

References

Allen, F., G. Almasi, W. Andreoni, D. Beece, B. J. Berne, A. Bright, J. Brunheroto, C. Cascaval, J. Castanos, P. Coteus, P. Crumley, A. Curioni, M. Denneau, W. Donath, M. Eleftheriou, B. Fitch, B. Fleisher, C. J. Georgiou, R. Germain, M. Giampapa, D. Gresh, M. Gupta, R. Haring, H. Ho, P. Hochschild, S. Hummel, T. Jonas, D. Lieber, G. Martyna, K. Maturu, J. Moreira, D. Newns, M. Newton, R. Philhower, T. Picunko, J. Pitera, M. Pitman, R. Rand, A Royyuru, V. Salapura, A. Sanomiya, R. Shah, Y. Sham, S. Singh, M. Snir, F. Suits, R. Swetz, W. C. Swope, N. Vishnumurthy, T. J. C. Ward, H. Warren, R. Zhou. 2001. Blue Gene: A vision for protein science using a petaflop supercomputer. *IBM Systems Journal*. 40:310

Allen, M. P.and D. J. Tildesley. 1987. Computer Simulation of Liquids. Oxford University Press, Oxford.

Birner, R., M. Bürgermeister, R. Schneiter, and G. Daum. 2001. Roles of Phosphatidylethanolamine and of Its Several Biosynthetic Pathways in *Saccharomyces cerevisiae*. *Mol. Bio. Cell*. 12:997-1007

Blume, A. 1980. Thermotropic Behavior of Phosphatidylethanolamine-Cholesterol and Phosphatidylethanolamine-Phosphatidylcholine-Cholesterol Mixtures. *Biochemistry*. 19:4908-4913

Böckmann, R. A., A. Hac, T. Heimburg, and H. Grubmüller. 2003. Effect of Sodium Chloride on a Lipid Bilayer. *Biophys. J*., 85:1647-1655

Brown, M. F., and J. Seelig. 1978. Influence of Cholesterol on the Polar Region of Phosphatidylcholine and Phosphatidylethanolamine Bilayers. *Biochemistry* 17:381-384

Emoto, K. and M. Umeda. 2000. An Essential Role for a Membrane Lipid in Cytokinesis: Regulation of Contractile Ring Disassembly by Redistribution of Phosphatidylethanolamine. *J. Cell Bio*. 149:1215-1224

Emoto, K., T. Kobayashi, A. Yamaji, H. Aizawa, I. Yahara, K. Inque, and M. Umeda. 1996. Redistribution of phosphatidylethanolamine at the cleavage furrow of dividing cells during cytokinesis. *Proc. Nat. Acad. Sci. USA*, 93:12867-12872

Epand, R. M. and R. Bottega. 1987. Modulation of the Phase Transition Behavior of Phosphatidylethanolamine by Cholesterol and Oxysterols. *Biochemistry*. 26:1820-1825

Dowen, W. 1997. Molecular basis for membrane phospholipids diversity: why are there so many lipids? *Annu. Rev. Biochem*. 66:199-232

Dufrêne, Y. F., W. R. Barger, J.-B. D. Green, and G. U. Lee. 1997. Nanometer-Scale Properties of Mixed Phospholipid Monolayers and Bilayers. *Langmuir*. 13:4779-4784

Feller, S. E., R. M. Venable, and R. W. Pastor. 1997. Computer Simulation of a DPPC Phospholipid Bilayer: Structural Changes as a Function of Molecular Surface Area. *Biophys. J.* 13:6555-6561

Feller, S. E. and R. W. Pastor. 1999. Constant surface tension simulation of lipid bilayers: The sensitivity of surface areas and compressibilities. *J. Chem. Phys*. 11:1281-1287

Fitch, B. G., R. S. Germain, M. Mendell, J. Pitera, M. Pitman, A. Rayshubskiy, Y. Sham, F. Suits, W. Swope, T. J. C. Ward, Y. Zhestkov and R. Zhou. 2003. Blue Matter, an application framework for molecular simulation on Blue Gene. *J. Para. Distrib. Comp*.63:759-773

Henneberry, A. L., M. M. Wright, and C. R. McMaster. 2002. The Major Sites of Cellular Phospholipid Synthesis and Molecular Determinants of Fatty Acid and Lipid Head Group Specificity. *Mol. Bio. Cell*. 13:3148-3161

Hitchcock, P.B., R. Mason, K. M. Thomas, and G. G. Shipley. 1974. Structural Chemistry of 1,2 Dilauryl-DL-phosphatidylethanolamine: Molecular Conformation and Intermolecular Packing of Phospholipids *PNAS*, 71:3036

Huber, T., K. Rajamoorthi, V. F. Kurze, K. Beyer, and M. F. Brown. 2002. Structure of Docosahexaenoic Acid-Containing Phospholipid Bilayers as Studied by ^{2}H NMR and Molecular Dynamics Simulation. *J. Am. Chem. Soc*., 124:298-309

Huster, D., K. Arnold, and K. Gawrisch. 2000. Strength of Ca^{2+} Binding to Retinal Lipid Membranes: Consequences for Lipid Organization. *Biophys. J.*, 78:3011-3018

Huster D., K. Arnold, and K. Gawrisch. 1999. Investigation of Kipid Organization in Biological Membranes by Two-Dimensional Nuclear Overhauser Enhancement Spectroscopy. *J. Phys. Chem. B.* 103:243-251

Huster, D., K. Arnold, and K. Gawrisch. 1998. Influence of Docosahexaenoic Acid and Cholesterol on Lateral Lipid Organization in Phospholipid mixtures. *Biochemistry*, 37:17299-17308

Hsieh, C. H. and W. G. Wu. 1995. Molecular order and hydration property of amine group in phosphatidylethanolamine and its N-methyl derivatives at subzero temperatures. Biophys. J. 69:2521-2530

Jahn, R. and H. Grubmüller. 2002. Membrane Fusion. *Curr. Opin. Cell. Biol*. 14:488-495

Kabsch, W. and C. Sander. 1983. Dictionary of protein secondary structures: Pattern recognition of hydrogen-bonded and geometrical features. *Biopolymers.* 22:2577-2637

Kearns, D. B., J. Robinson, and L. J. Shimkets. *Pseudomonas aeruginosa* Exhibits Directed Twitching Motility Up Phosphatidylethanolamine gradients. 2001. *J. Bacteriology* 183:763-767

Kozlov, M. M., S. Leikin, and R. P. Rand. 1994. Bending, Hydration , and Interstitial Energies Quantitatively Account for the Hexagonal-Lameller-Hexagonal Reentrant Phase Transition in Dioleoylphosphatidylethanolamine. *Biophys. J.* 67:1603-1611

Martinez, P., and A. Morros. 1996. Membrane Lipid Dynamics During Hyman Sperm Capacitation. *Frontiers in Bioscience*. 1:103-117

Mashi, R. J., H. L. Scott, S. Subramaniam, and E. Jakobson. Molecular Simulation of Dioleoylphosphatidylcholine Lipid Bilayers at Differing LLevels of Hydration. *Biophys. J*. 81:3005-3015

Moore, P. B, C. F. Lopez, and M. L. Klein. 2001. Dynamical Properties of a Hydrated Lipid Bilayer from a Multinanosecond Molecular Dynamics Simulation. *Biophys. J.* 81:2484-2494

Nagle, J. F. 1993. Area/lipid of bilayers from NMR. *Biophys. J.* 64:1476-1481

Paré, C., M. Lafleur. 1998. Polymorphism of POPE/Cholesterol System: A ^{2}H Nuclear Magnetic Resonance and Infrared Spectroscopic Investigation. *Biophys. J.* 74:899-909

Petrache, H., K. Tu, and J. F. Nagle. 1999. Analysis of Simulated NMR Order Parameters for Lipid Bilayer Structure Deremination. Biophys. J. 76:2479-2487

Phillips, M. C., H. Hauser, and F. Paultauf. 1972. *Chem. Phys. Lipids*. 8:127

Rappolt, M., A. Hickel, F. Bringezu, and K.Lohner. 2003. Mechanism of the Lamellar/ Inverse Hexagonal Transition Examined by High Resolution X-Ray Diffraction. *Biophys. J*. 84:3111-3122

Rand, R.P., and V.A. Parsegian. 1989. Hydration Forces Between Phospholipid Bilayers. *Biochimica et Biophysica Acta*. 988:351-376

Rawicz, W., K. C. Olbrich, T. J. McIntosh, D. Needham, E. A. Evans. 2000. Effect of Chain Length and Unsaturation on Elasticity of Lipid Bilayers. *Biophys. J.* 79:328-373

Saiz, L. and M. Klein. 2001a. Influence of Highly Polyunsaturated Lipid Acyl Chains of Biomembranes on the NMR Order Parameters. *J. Am. Chem. Soc*. 123:7381-7387

Saiz, L. and M. Klein. 2001b. Structural Properties of a Highly Polyunsaturated Lipid Bilayer from Molecular Dynamics Simulation. Biophys. J., 81:204-216

Seelig, J. and Nada Waespe-Šarčević, 1978. Molecular Order in Cis and Trans Unsaturated Phospholipid Bilayers. *Biochemistry*. 17:3310-3315

Seelig, A. and J. Seelig 1977. Effect of a Single Cis Double Bond on the Structure of a Phopholipid. *Biochemistry* 16:45-50

Seelig, J. and A. Seelig 1980. Lipid conformation in model membranes and biological membranes. *Quarterly Reviews in Biophysics* 13:19-61

Story, M. K., K. L. Clay, T. Kutateladze, R. C. Murphy, M. Overduin, and D. R. Voelker. 2001, Phosphatidylethanolamine Has an Essential Role in *Saccharomyces cerevisiae* That is Independent of Its Ability to Form Hexagonal Phase Structures. *J. Bio. Chem*. 276:48539-48548

Teague, W., N. L. Fuller, R. P. Rand, and K. Gawrisch. 2002. Polyunsaturated Lipids in Membrane Fusion Events. *Cell. Mol. Biol. Lett*. 7:262-264

Weiner, M. C. and S. White. 1992. Structure of a fluid dioleoylphosphatidylcholine bilayer determined by joint refinement of x-ray and neutron diffraction data III. Complete structure. *Biophys. J*. 61:434-447

Weiss, J. A., D. W. Oxtoby, and D. G. Grier. 1995. Martensitic transition in a confined colloidal suspension. *J. Chem. Phys*. 103:1180-1190

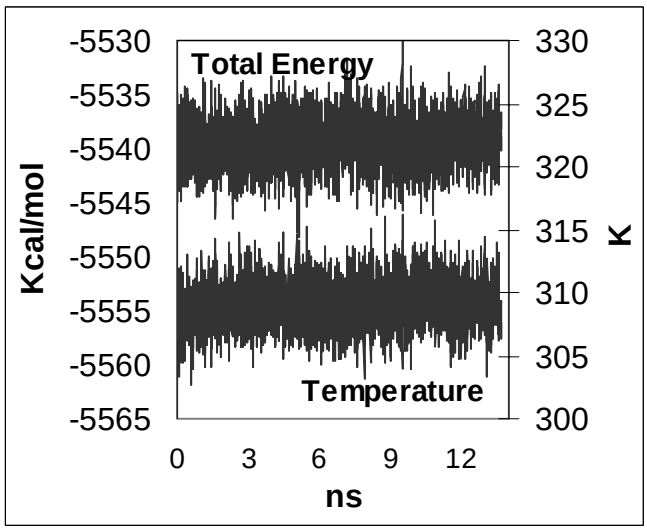

Figure 1

Energy and temperature trace over the duration of the 14 ns microcanonical production run. The remarkable stability resulted from standard Verlet integration with 2fs timestep. Long range electrostatics were calculated using P3ME at every timestep, with a 0.5 Å mesh (see methods). The slope of the least-squares trend line for the total energy is 0.03 Kcal/mol per ns, and is small on the scale of the long term oscillations. The temperature trace over the duration of the run also shows long term oscillations with multi-nanosecond periods. The slope of the least squares trend line is 0.03 degrees per ns, and is similarly small compared to the long term oscillations.

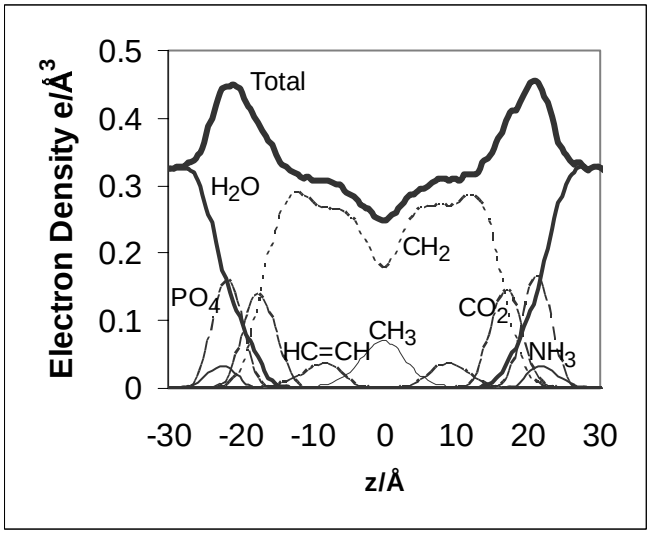

Figure 2

Electron density distribution with respect to the bilayer normal. The total electron density from simulation is shown in bold, along with the contributions from selected groups. Note the broad distribution of the terminal methyl groups extending almost up to the acyl The likelihood of occurrence for surface exposure in bulk is perhaps less than a weighting of 1/72 would imply (see text for discussion).

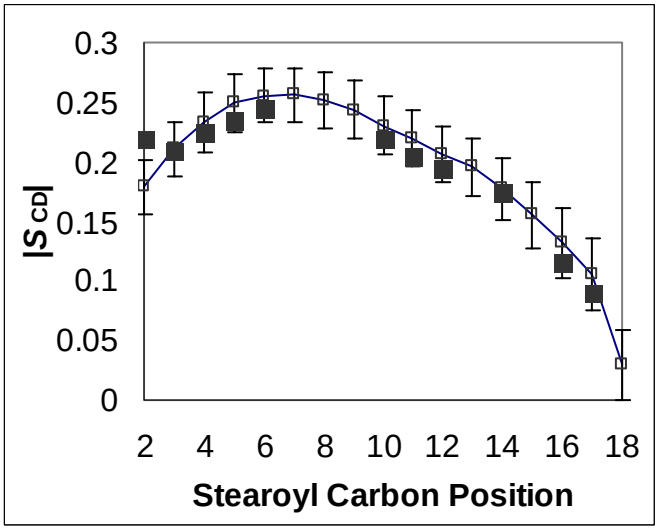

Figure 3

Comparison of stearoyl chain simulated order parameter profile (open squares with connecting lines as a visual aid) to the selectively deuterated palmitoyl POPC order parameters (Filled squares – data from Seelig and Seelig, 1977). To properly compare the stearoyl chain to the palmitoyl chain, the plateau and the tail regions were aligned separately. See text for details.

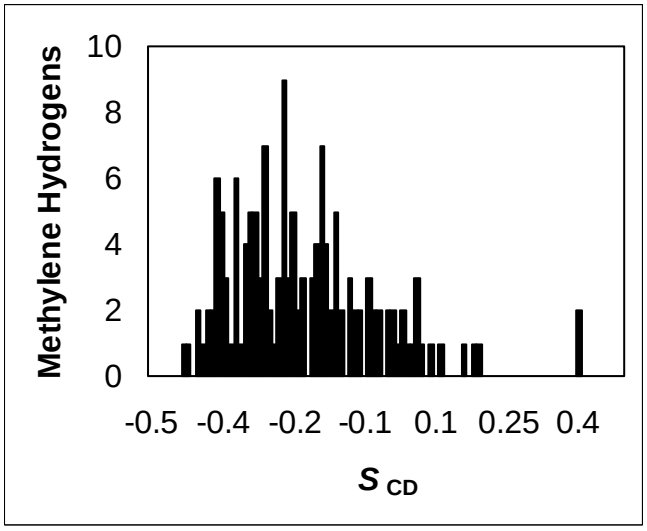

Figure 4

Histogram of the S_{CD} for the methylene hydrogens in the C2 position of the stearoyl chain. The distribution is skewed toward disorder with two clear outliers. Inspection of the chain conformation for the two outliers reveals surface exposure of the stearoyl chain. The likelihood of occurrence for surface exposure in bulk is perhaps less than a weighting of 1/72 would imply (see text for discussion).

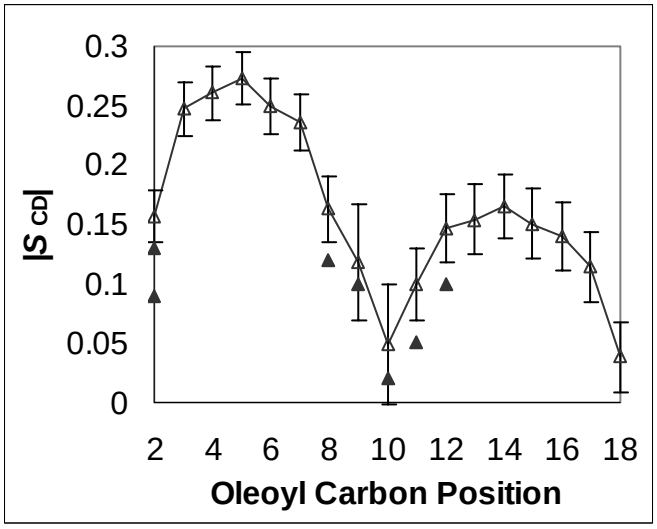

Figure 5

Comparison of oleoyl chain simulated order parameter profile (open triangles) to the selectively deuterated oleoyl POPC order parameters (filled triangles – data from Seelig and Seelig, 1977). The characteristically low order parameters around the double bond (carbons 9 and 10) agree well. The nonequivalent methylenes at the C2 position are not seen in simulation, although the simulated C2 methylenes do have considerably lower values than other plateau region methylenes. Values where selective deuteration was not reported compare well to corresponding carbons on stearoyl chain (see Figure 4).

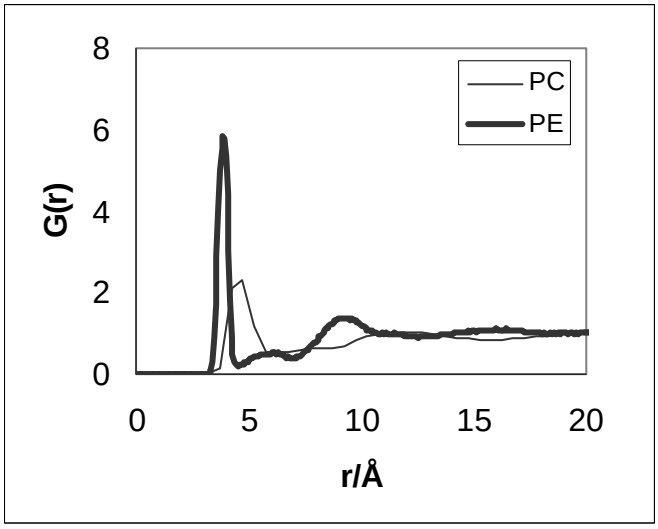

Figure 6

Inter-molecular phosphorous-nitrogen two-dimensional radial distribution function for PE (thick line) and PC (thin line). Hydrogen bonding between the amine and the phosphate groups laterally organizes PE much more than the more weakly associated phosphate choline interactions in PC. The structure extends over a longer range, indicating a degree of clustering not observed in PC simulations.

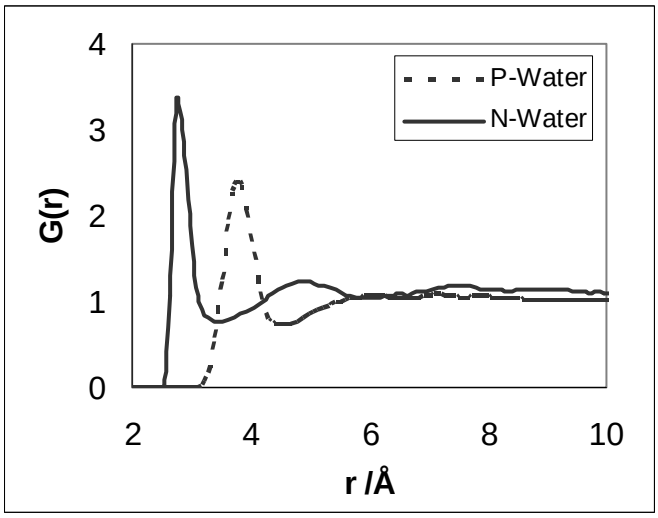

Figure 7

Phosphorous-water and nitrogen-water three-dimensional radial distribution functions. Hydration of the primary amine is pronounced and evident out to three solvation shells. Solvation structure around the phosphate is much less structured, becoming effectively random after the first solvation shell. The phosphate and amine groups compete for hydrogen bonds with each other and with water.

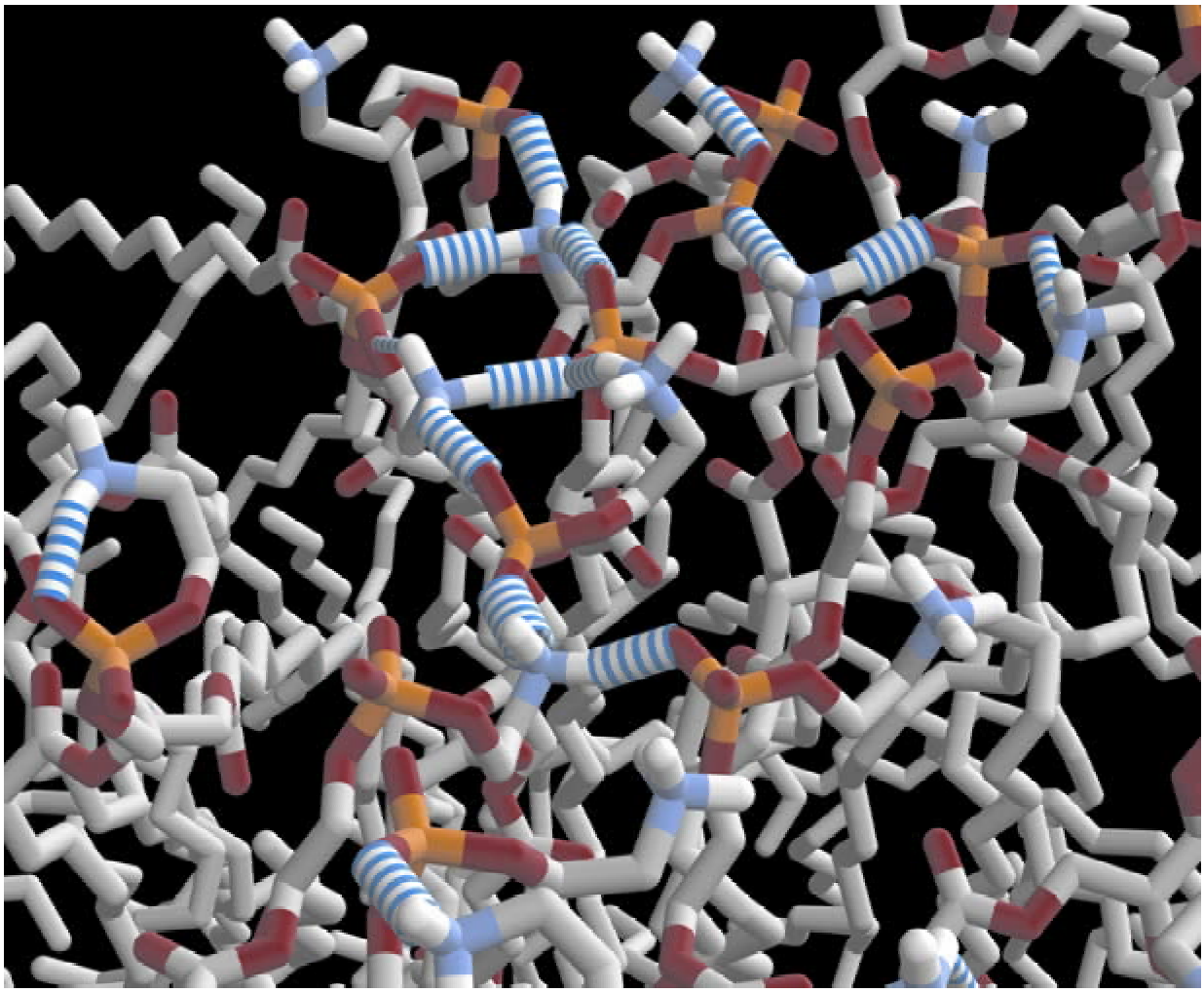

Figure 8

Snapshot depicting the extent of hydrogen bond networks on the surface. A rich variety of coordination modes are evident including mono- and bi-furcated hydrogen bonding of amine and phosphate oxygens, and mono-, bi-, and tri-fold coordination of amine and phosphate groups. Such high branching factors enable the formation of extensive hydrogen bond networks.

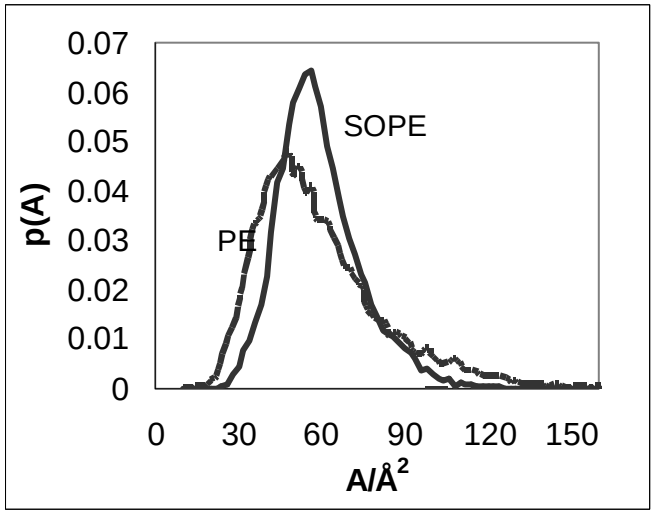

Figure 9

Area per lipid distribution from Voronoi cells tessellating both the center of mass of the SOPE (COM_{SOPE}), and the center of mass of only the phosphoethanolamine portion of the headgroups (COM_{PE}). Each distribution was computed from 50ps snapshots over the 14ns of simulation time. The mean for COM_{SOPE} is 58.2 $Å^2$ with r = 14.8; the mean for tessellating with just the PE is necessarily the same, while r = 22.4, implying a lower compressibility modulus. These values correspond to a lateral compressibility modulus of $K_{A(SOPE)}$ = 113 dyn/cm and $K_{A(PE)}$ = 49.8 dyn/cm. Note the distributions are skewed toward higher areas ($skew_{SOPE}$ = 0.80, $skew_{PE}$ = 1.16).

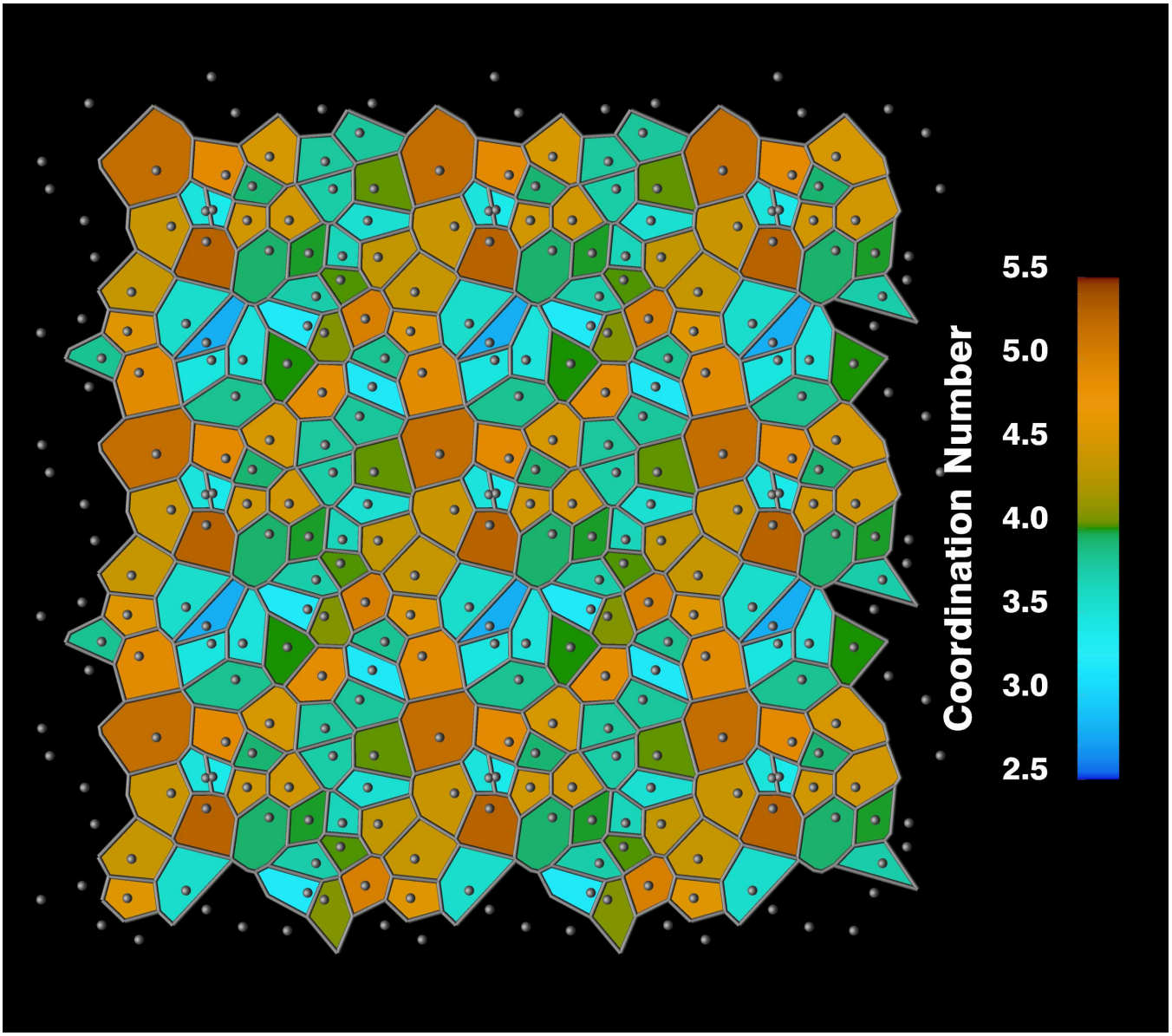

Figure 10

Voronoi tessellation for the center of mass of the phosphoethanolamine groups for a sample snapshot. Nine simulation cells are shown. The color coding indicates the coordination number as defined by Weiss et al. 1995. Regions of high and low head group density are laterally organized and generally extend into the symmetry-related neighboring cells. The larger area Voronoi cells tend to group together, representing regions of low headgroup density or boundary regions of a cluster. The lateral organization is fairly dynamic, yet many local coordination motifs are stable on the nanosecond timescale.

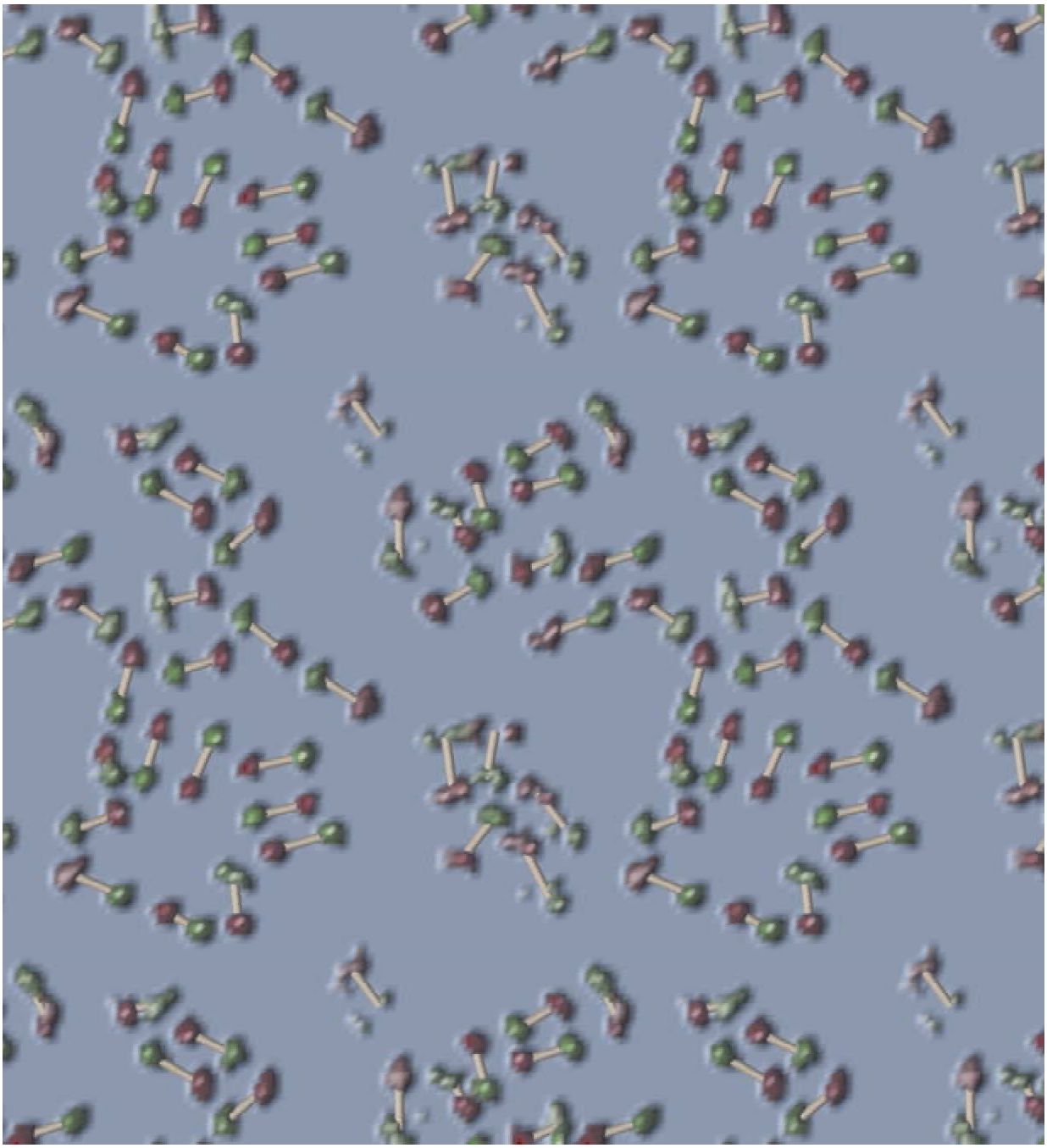

Figure 11

Time average of the phosphate (red) and Nitrogen (green) positions over the 100ps time window beginning with the Voronoi tessellated configuration shown in Figure 10. The tubes connecting each phosphate distribution with a corresponding nitrogen distribution indicate the P-N pairs in the same lipid. The width of the distributions indicates the positional distribution over a 100ps time frame. Four simulation cells are shown. Hydrogen bond networks between amine and phosphate groups are evident in the patterns of alternating red and green density clouds. Over this time window an individual lipid (and three symmetry equivalents) can be seen in an unbound migratory state where the N distribution is bimodal and the P distribution is relatively diffuse. Other motifs such as rings are apparent, as well as centrally radial coordinations (see Fig. 12 for a detailed view).

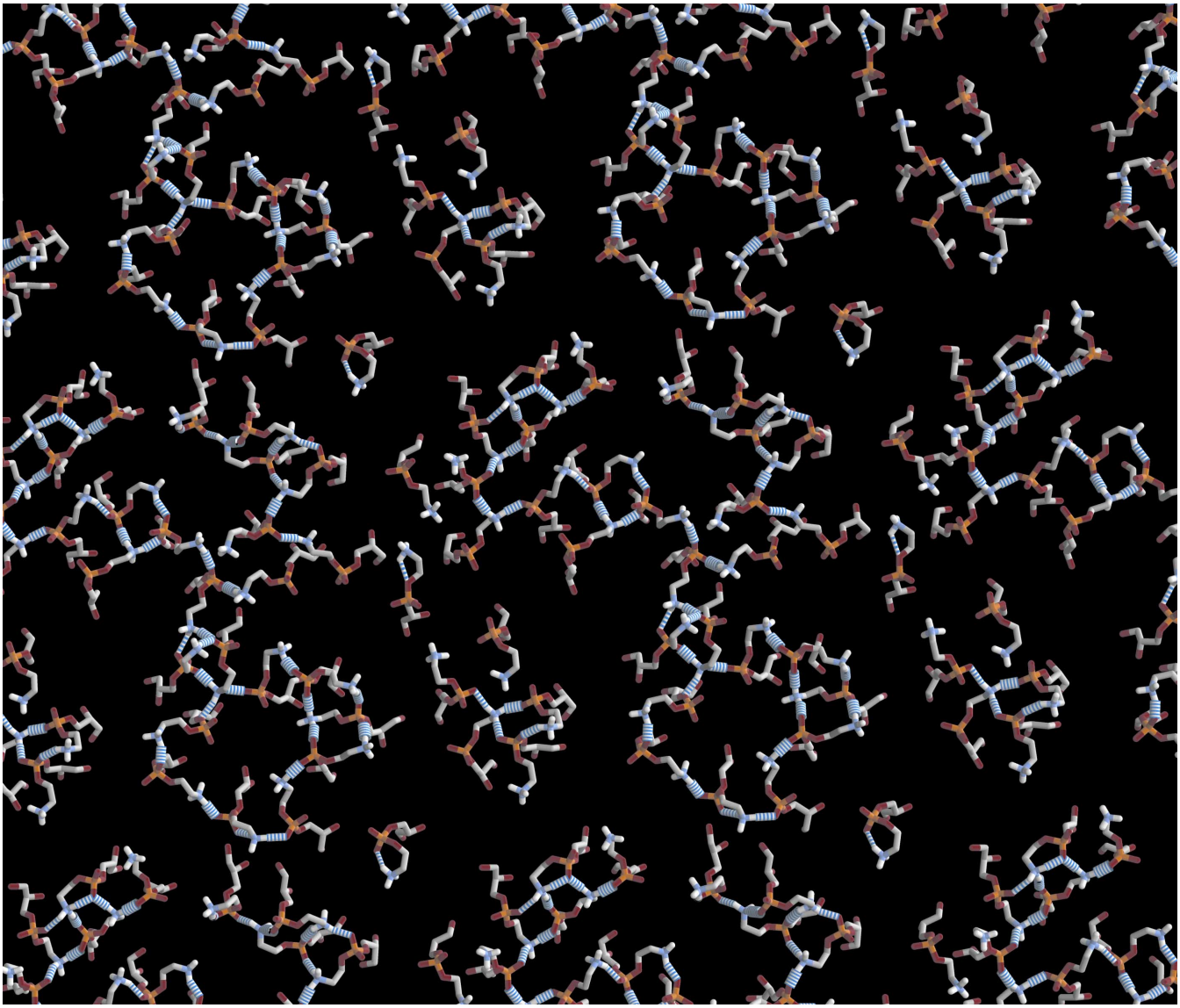

Figure 12

Detailed atomic view of the headgroups corresponding to Figures 10 and 11. Here the atoms of the phosphatidylethanolamine are shown with explicit hydrogen bonding rendered as blue striped cylinders. The rich variety of hydrogen bonding patterns clearly support the higher level of organizational motifs apparent in Figures 10 and 11.